ACS APPLIED MATERIALS & INTERFACES

Research Article

www.acsami.org

Passivated Aluminum Nanohole Arrays for Label-Free Biosensing Applications

Víctor Canalejas-Tejero,[†] Sonia Herranz,[‡] Alyssa Bellingham,[§] María Cruz Moreno-Bondi,[‡] and Carlos Angulo Barrios*[,†]

[†]Instituto de Sistemas Optoelectrónicos y Microtecnología (ISOM), ETSI Telecomunicación, Universidad Politécnica de Madrid, CEI-Moncloa, 28040 Madrid, Spain

[‡]Chemical Optosensors and Applied Photochemistry Group (GSOLFA), Department of Analytical Chemistry, Faculty of Chemistry, Universidad Complutense, CEI-Moncloa, 28040 Madrid, Spain

[§]Department of Electrical and Computer Engineering, Drexel University, 3141 Chestnut Street, Bossone Research Enterprise Center Suite, Philadelphia, Pennsylvania 19104, United States

ABSTRACT: We report the fabrication and performance of a surface plasmon resonance aluminum nanohole array refractometric biosensor. An aluminum surface passivation treatment based on oxygen plasma is developed in order to circumvent the undesired effects of oxidation and corrosion usually found in aluminum-based biosensors. Immersion tests in deionized water and device simulations are used to evaluate the effectiveness of the passivation process. A label-free bioassay based on biotin analysis through biotin-functionalized dextran−lipase conjugates immobilized on the biosensor-passivated surface in aqueous media is performed as a proof of concept to demonstrate the suitability of these nanostructured aluminum films for biosensing.

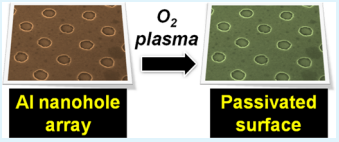

KEYWORDS: *aluminum, biosensor, nanoholes, oxidation, surface passivation*

INTRODUCTION

After nearly a century since the first observations of visible light coupling with collective oscillations of free electrons in a conductor material by Wood, who saw unexplained light diffraction coming from metallic gratings,[1] and decades after the first approach to subwavelength holes in a metal,[2] Ebbesen and co-workers showed the extraordinary optical transmission (EOT) through metallic subwavelength hole arrays.[3−5] The mentioned electronic oscillations are known as surface plasmons (SPs), which is a term introduced in 1956 by Pines.[6] Surface plasmon polaritons (SPPs) are electromagnetic excitations at the metal/dielectric interface that can be exploited for several uses[7,8] as photonic devices; subwavelength, nonlinear, and near-field optics; optical recording; visible and Raman spectroscopy; solar cells; chemical sensors; and biosensors. Surface plasmon resonance (SPR) is the way to implement SPs in real applications by means of tools such as prism or grating coupling,[9,10] or nanostructured features[11] as nanoparticles and nanoholes.

Optical techniques based on SPR have been shown to be successful for biosensing applications[12−16] and can even be attached to modern cell phones,[17] showing big opportunities for in situ, worldwide health or environmental sensing and diagnostics. Metallic nanostructures provide new design and integration possibilities, which can lead to improvements in key SPR-based biosensor issues, such as sensitivity, resolution, multiplexing, and biological interfacing. Light transmission through subwavelength hole arrays has been extensively studied and discussed.[18−29] Nanohole-array-based chemical and biological sensors offer numerous applications and display great performance,[30−40] and recent progress has been focused on less-expensive fabrication methods.[41,42] SPR sensitivity to the dielectric materials in contact with the metal surface is the key for sensing applications,[43] and it can be optically measured as refractive index (RI) changes reflected in spectral feature shifts or intensity variations.[44]

Noble metals such as gold and silver are used in the fabrication of the vast majority of nanohole-array SPR devices,[45,46] because of their very low resistivity, translated into low optical losses in the visible and near-infrared ranges. Gold is highly stable chemically, making this metal convenient for biological media, whereas silver has poorer environmental stability, which can be solved by depositing an overlayer of alumina via atomic layer deposition.[47,48] However, the high cost of these metals limits large-scale commercialization of these sensors. A more cost-effective plasmonic material is aluminum, which is ∼25 000 times less expensive than gold and ∼425 times less expensive than silver, as of September 2013.[49] Despite this observation, aluminum has been scarcely considered for the implementation of SPR biosensors, mainly because of challenges from oxidation and material degradation (corrosion and pitting).[50−52]

The passivation of aluminum is a well-known phenomenon that involves the oxidation of the exposed-to-air aluminum surface into a thin, insulating, water-insoluble and waterproof film that is able to resist reactions with water, oxygen, or diluted

Received: October 13, 2013
Accepted: December 20, 2013
Published: December 20, 2013

   dx.doi.org/10.1021/am404509f | ACS Appl. Mater. Interfaces 2014, 6, 1005−1010

acids.[53] The formation of an oxide layer thus protects the inner aluminum and inhibits further oxidation reactions. However, native aluminum oxide (2−3 nm thick[50]) is usually not enough to avoid progressive oxidation and corrosion in aluminum thin films (≤100 nm)—typically deposited on substrates via evaporation or sputtering techniques—in which the existence of microdefects, nanodefects, and nanopores is frequent.

In this paper, we show that aluminum can be made a suitable and reliable plasmonic material for implementing nanohole-array SPR biosensors. The issue of aluminum oxidation is tackled by means of a passivation process consisting of exposing aluminum nanohole-array films to an oxygen-gas (O_2) plasma. This treatment produces a robust oxide protective layer that is more resistant than native oxide against oxidizing agents such as aqueous solutions or buffers usually employed in biosensing tests, thus avoiding corrosion and pitting issues. We report a competitive immunoassay to demonstrate the workability of our aluminum nanohole arrays as optically interrogated biosensors.

EXPERIMENTAL SECTION

Nanohole Array Fabrication. Glass substrates 1 mm thick were thoroughly washed with detergent in an ultrasonic aqueous bath, cleaned using piranha solution (H_2SO_4 (96% purity) + H_2O_2 (30%) 3:1 at 130 °C), rinsed in deionized water (DIW) and isopropyl alcohol (IPA), blown-dry with N_2 flow, and heated at 100 °C for 10 min. Then, a 100-nm-thick layer of aluminum was deposited on the glass substrates by electron-beam evaporation. Next, ZEP-520 positive-tone electron beam lithography (EBL) resist was spin-coated on the aluminum film at 5000 rpm and immediately baked for 10 min at 120 °C. 500-nm-pitch two-dimensional (2D) arrays of dots were patterned in the resist film by e-beam single-shot exposure, using a Crestec CABL-9000C high-resolution EBL system (acceleration voltage = 50 keV, beam current = 1 nA, exposure time = 200 μs). The exposed resist was developed at 0 °C over 40 s and then dried using a N_2 flow. Inductively coupled plasma (ICP) chemical dry etching was used to drill holes in the aluminum layer down to the glass substrate using the patterned ZEP-520 film as a mask. The ICP process was achieved using BCl_3 (20 sccm) and Cl_2 (10 sccm) gases, and RF and ICP power of 100 W for 35 s. The etch selectivity of aluminum over the resist was 1.18:1, which leads to an almost-complete removal of the resist mask after etching. Immediately after the ICP etch, the samples were rinsed in DIW for 5 min to dissolve residual Al_2Cl_3. An O_2 plasma ashing (RF power = 30 W; O_2 flow = 15 sccm) was carried out for 5 min. Figure 1 shows a scanning electron microscopy (SEM) photograph of a fabricated Al nanohole array; the resulting diameter of holes was ∼220 nm. Finally, a surface passivation process of the nanostructured Al films consisting of O_2 plasma exposure (RF power = 80 W; O_2 flow = 15 sccm) for times ranging from 5 min to 60 min was achieved.

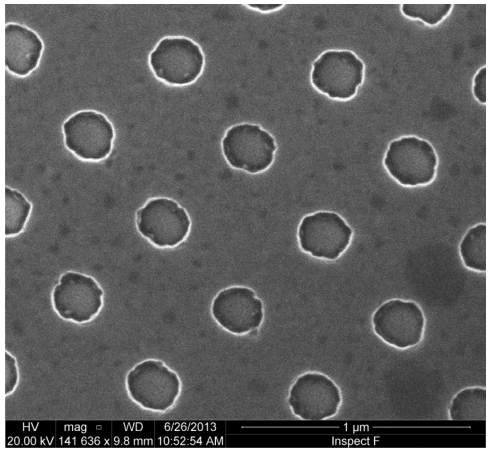

Figure 1. Scanning electron microscopy (SEM) micrograph of a fabricated aluminum nanohole grating.

Aluminum Wet Oxidation and Bulk Sensing Experiments. The effect of the exposure of the aluminum devices to an aqueous environment was studied by immersing the samples in DIW (pH 5.7) for 30-min intervals up to a maximum of 16 h. After each 30-min-long immersion, the samples were rinsed with IPA for 10 s and dried with N_2 flow, and their transmission spectra were measured by means of a Jasco V-650 UV-VIS spectrophotometer, using unpolarized light under normal incidence in the 500−850 nm wavelength range and a spectral resolution of 0.1 nm. Collected data was smoothed using the means-movement method (convolution width of 13). Bulk refractive index (RI) sensing tests were performed by immersing passivated samples in a variety of solvents (methanol (RI = 1.3303), DIW (RI = 1.3334), acetone (RI = 1.3602), ethanol (RI = 1.3624), IPA (RI = 1.3777), tetrahydrofuran (RI = 1.4085), cyclohexane (RI = 1.4277), and toluene (RI = 1.4972)) inside a quartz cuvette and measuring the corresponding spectral transmission as previously described. The RI values of the solvents were measured with a Krüss Model DR201-95 refractometer.

Antigen Immobilization onto the Sensing Surface. Passivated aluminum nanohole arrays were functionalized with 1,1,1,3,3,3-hexamethyldisilazane (HMDS), obtained from Sigma (St. Louis, MO, USA), by placing a 10-μL droplet on the array surface and allowing a cleaned glass slide to fall down onto the droplet to prevent evaporation. After 16 h of reaction at room temperature (RT), glass covers were removed and the aluminum nanohole arrays were rinsed three times in hexane (to remove the unbound silanizing reagent) and dried with argon.

Biotin−dextran−lipase conjugates, prepared as described previously,[54] were hydrophobically adsorbed onto the HMDS-functionalized Al nanohole arrays by placing them upside down in contact with 150 μL of an aqueous solution of the conjugate (100 μg mL^{-1}) in a polypropylene container. After 10 min of incubation at RT, the aluminum nanohole arrays were rinsed three times in Milli-Q water to remove unbound conjugate and dried with argon.

Bioassay Protocol. The measuring principle was based on a competitive inhibition assay between the biotin−dextran−lipase conjugates immobilized onto the aluminum nanohole array surface and biotin present in the sample solution for a limited number of anti-biotin antibody (Ab) binding sites.

For direct assay, 0.2 μg mL^{-1} anti-biotin Ab solution (150 μL, in 10 mM HEPES at pH 7.4) was incubated with the conjugate-derivatized array (60 min at RT). For competitive inhibition assays, 140 μL of the biotin standard solution in 10 mM HEPES at pH 7.4 (final concentration of 2 μg mL^{-1}) was mixed with 10 μL of 3 μg mL^{-1} anti-biotin Ab solution (final concentration of 0.2 μg mL^{-1}), pre-incubated for 5 min at RT followed by incubation with the aluminum nanohole arrays for 60 min at RT.

Finally, the arrays were rinsed three times in Milli-Q water and the amount of anti-biotin Ab bound to the array surface was evaluated by measuring the visible transmission spectra. In order to study the repeatability of the process, the direct and competitive assays were carried out in triplicate.

THEORETICAL CALCULATIONS

The transmission spectrum of an aluminum nanohole square lattice was calculated using the finite-difference time-domain (FDTD) algorithm.[55] The simulated device geometry consisted of a 500-nm-period 3 × 3 array of cylindrical holes 220 nm in diameter in a (100 − t_{ox})-nm-thick layer of aluminum on a bottom glass substrate, where t_{ox} is the thickness of a conformal Al_2O_3 layer on the grating sensing surface. The frequency-dependent dielectric constant of aluminum was modeled by the well-known Drude−Lorentz equation with the fitted parameters reported in the literature.[45] The dielectric constants of glass and Al_2O_3 were assumed to be frequency-independent and

equal to 2.32 and 3.15, respectively. Periodic boundary conditions were chosen along the device plane coordinates (x- and y-axis of the array) and perfectly matched layer (PML) boundary condition was used along the incident-beam propagation direction (z-axis), normal to the device plane. Frequency analysis of the transmission was achieved by launching a pulsed excitation from the glass substrate towards the aluminum array and calculating the fast Fourier transform (FFT) of the time-domain field component (E_x) on a plane above the holes.

RESULTS AND DISCUSSION

Calculated and measured visible spectra of aluminum nanohole arrays in air are shown in Figure 2. The simulated spectrum

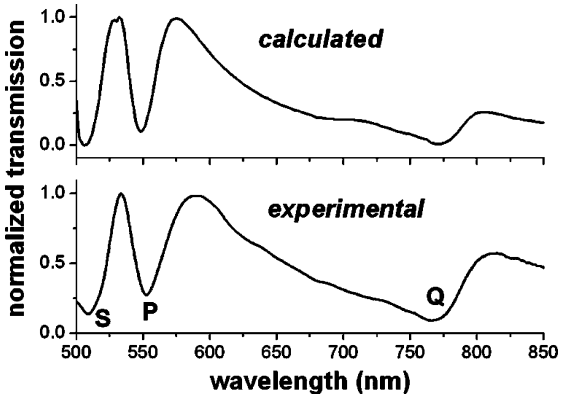

Figure 2. Experimental and calculated visible spectra of an aluminum nanohole array with pitch = 500 nm, aluminum thickness = 100 nm, and hole diameter = 220 nm.

corresponds to a device with no oxide layer (t_{ox} = 0), whereas the experimental curve stands for a non-passivated grating. Good agreement between calculations and experimental data is observed, supporting the validity of our FDTD model. Three main resonance features are seen and referred to as their respective minima: S-wavelength (~507 nm), P-wavelength (~550 nm), and Q-wavelength (~770 nm). The SPP grating-coupling equation,

$$\lambda_{SPP} \approx \frac{a}{\sqrt{i^2 + j^2}} \sqrt{\frac{\varepsilon_d \varepsilon_m}{\varepsilon_d + \varepsilon_m}} \quad (1)$$

where a is the array period, i and j are grating orders, and ε_m and ε_d are the dielectric functions of the metal and dielectric medium, respectively, predicts SPP resonances at 507 nm for i = ±1, j = 0 (or vice versa) for the metal/air interface and 553 nm for i = ±1, j = ±1 and 771 nm for i = ±1, j = 0 (or vice versa) for the metal/glass interface, which also fits well with both the experimental and simulated resonance peaks. Therefore, we attribute the observed resonances to SPPs. Since the S-peak wavelength (λ_S) is dependent on the dielectric constant of air—and, therefore, that of whichever medium is replacing air—λ_S shifts will be used to monitor the sensor response. An increase of the medium RI (e.g., because of the adsorption of a thin film onto the device surface) should result in a λ_S red shift, whereas a decrease of the medium index (e.g., due to a removal of a thin film on the device surface) should lead to a λ_S blue shift.

Effect of Passivation Treatment. Figure 3 shows the variation of λ_S for Al gratings passivated for different times,

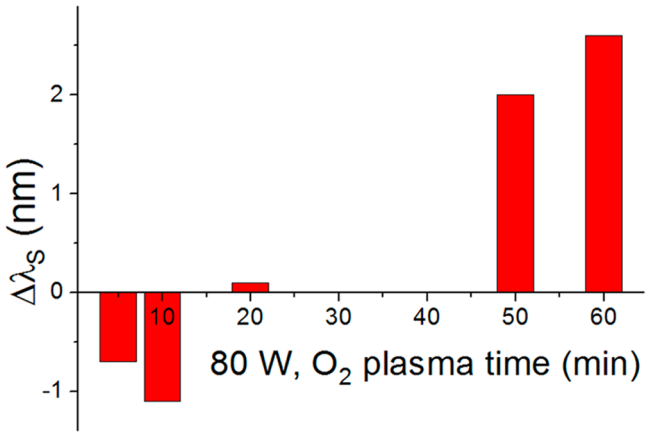

Figure 3. S-wavelengths shifts for passivation times of 5, 10, 20, 30, 40, 50, and 60 min.

compared to that of a non-passivated device. λ_S blue-shifts for short plasma times (5−10 min), which is attributed to the removal of ZEP-520 resist residues. For passivation times of ≥50 min, red-shifts of a few nanometers are observed, which are attributed to a thickness increase of a superficial aluminum oxide layer. This is supported by simulations, which indicate a rate of $\Delta\lambda_S/\Delta t_{ox}$ = 1 nm/nm (for the sake of comparison, the latter value is consistent with the results obtained by other groups on alumina-overlayer thickness sensitivity of silver nanohole arrays[56]). Note that no significant shifts are seen for plasma times lasting between 20 min and 40 min. The existence of a pre-passivation native oxide film, acting as a diffusing barrier for the O^{2-} ions, can explain this behavior. For longer plasma times, the ions are able to cross the oxide barrier and then react with aluminum, forming additional oxides, as previously mentioned.

Oxidation in DIW. Photographs in Figure 4 illustrate aluminum film degradation with DIW immersion time. As-deposited aluminum layers were passivated for times ranging from 0 to 60 min and immersed in DIW for 8 days. It is observed that (i) the native oxide of non-passivated Al films is not enough to prevent Al degradation and (ii) Al pitting is significantly reduced for plasma times of ≥10 min, setting a minimum passivation duration for the devices.

Figure 5 shows the variation of the S-wavelength with the immersion time in DIW for aluminum nanohole arrays passivated for different time intervals. According to the calculated $\Delta\lambda_S/\Delta t_{ox}$ = 1 nm/nm, the oxidation rates can be estimated to be 0.249, 0.159, 0.096, 0.084, and 0.022 nm/h for 0, 5, 20, 40, and 60 min of oxygen-gas plasma treatment, respectively. That is, the oxidation rate decreases as the passivation time increases, demonstrating the protective function of the passivated surface against further oxidation.

Typical resonance-wavelength variations in metal nanohole array biosensors are on the order of 1 nm,[57−60] and exposure times to aqueous solutions of these sensors during incubation and recognition steps are usually not longer than 30 min. Therefore, passivation times of 40 min or longer should be sufficient to ensure reliable biosensing measurements in a variety of aqueous buffer solutions. However, note that passivation times longer than 40 min result in an increase of the oxide film (see Figure 3), which would decrease the sensitivity of the nanohole array, since the maximum sensitivity is achieved at the metal/dielectric media interface. Therefore, it is concluded that a passivation time between 40 min and 50

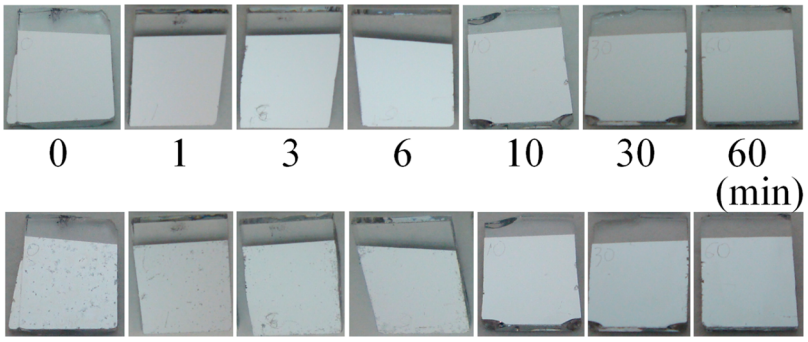

Figure 4. Corrosion test after different O_2 plasma times at 80 W and 15 sccm flow. Upper row shows 100-nm aluminum films on glass substrates before the test; lower row shows the same samples after 8 days of immersion in DIW. Left to right: 0, 1, 3, 6, 10, 30, and 60 min of O_2 plasma passivation. From 10 min onward, immersed samples do not show any noticeable corrosion or pitting to the naked eye.

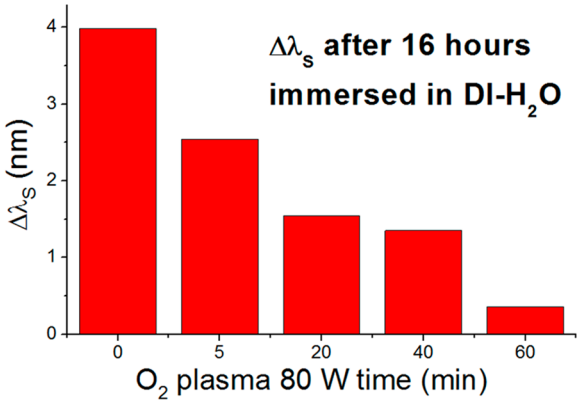

Figure 5. S-wavelength variation for five samples treated with different oxygen-gas (O_2) plasma times after 16 h of immersion in DIW in 30-min immersion steps.

min should be chosen to achieve both high resistance to corrosion and oxidation and high sensitivity.

Bulk Sensing. Figure 6 shows the recorded transmission spectra of a passivated aluminum nanohole array immersed in liquids having different RIs. The measured values of the S-wavelength as a function of the liquid RI are plotted in the inset, including the air case (n = 1). The sensor response is highly linear (the adjusted corelation coefficient (R^2) is 0.99983) over a wide range of RI values with a bulk sensitivity

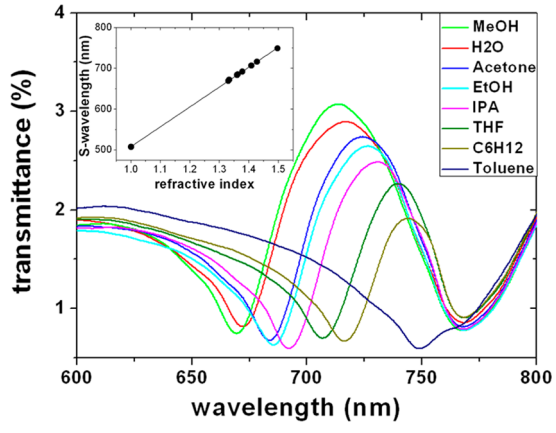

Figure 6. Experimental spectra of an aluminum nanohole grating immersed in liquids with different RIs. Inset shows S-wavelength as a function of the fluid RI, including air (n = 1).

of $S_B = d\lambda/dn$ = 487 nm/RIU. Device simulations indicate bulk sensitivities of 505 for t_{ox} = 0 and 501 nm/RIU for t_{ox} = 5 nm, showing that a thin oxide film does not affect the RI sensitivity of the aluminum nanohole array significantly. The discrepancy between experimental and calculated values can be due to device imperfections (roughness, non-vertical hole sidewalls) and/or material dispersion differences between real and modeled materials. For the sake of comparison, similar bulk sensitivities have been reported for a 500-nm-period silver nanohole array[56] (494 nm/RIU) and a 520-nm-period gold nanohole array[36] (393 nm/RIU).

Biosensing. Figure 7 shows the measured spectral shifts of S-wavelength for the different samples and tests carried out to

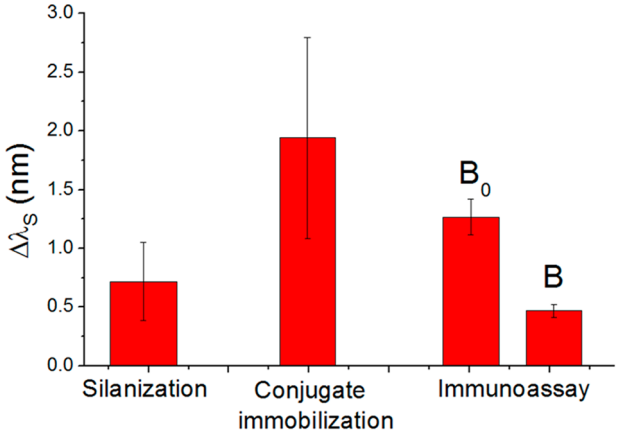

Figure 7. S-wavelength red-shifts measured after silanization, conjugate immobilization, direct assay (B_0), and competitive assay (B) experiments. The direct-assay red shift is ~3 times greater than that of the competitive assay.

prove the feasibility of performing immunoassays with the Al nanohole array devices. Red shifts for silanization and conjugate immobilization steps resulted from 11 and 10 replicas, respectively. In all cases, significant red shifts are measured for both silanization and receptor immobilization processes. This indicates the formation of the corresponding adlayers on the device surface that constitute the receptor elements of the biosensors. In the direct assays (B_0 samples), antibody recognition is also revealed as red shifts, which are clearly higher than those obtained for the competitive assays (B samples), as expected. After three replicas, processed individually for each assay, good relative standard deviation

dx.doi.org/10.1021/am404509f | ACS Appl. Mater. Interfaces 2014, 6, 1005−1010

(RSD) values were obtained: B_0-RSD = 12.1% and B-RSD = 12.4%.

Noted that, despite the several incubations in aqueous solutions involved in these experiments, no evidence of aluminum degradation was detected in the devices throughout the entire series of experiments. This supports the effectiveness of our passivation treatment.

CONCLUSIONS

Aluminum nanohole array refractometric biosensors have been fabricated and demonstrated. An aluminum surface passivation treatment, based on an oxygen-gas (O_2) plasma, has been developed to deal with the corrosion and pitting problems usually found in nanometric aluminum layers that have been exposed to oxidizing agents. This treatment produces an oxide protecting layer that is more resistant than native oxide exposed to the same chemical conditions. The passivation time has been optimized to obtain both good device resistance against pitting and oxidation and good refractive index sensitivity. The devices have been successfully tested as label-free optical biosensors using the biotin−dextran−lipase system, providing reliable results and showing no sign of aluminum degradation. Good performance and low cost—aluminum is 25 000 times less expensive than gold—make the presented SPR-based device a promising candidate for mass-produced label-free optical biosensors on chips.

AUTHOR INFORMATION

Corresponding Author

*E-mail: carlos.angulo.barrios@upm.es.

Notes

The authors declare no competing financial interest.

ACKNOWLEDGMENTS

The authors gratefully acknowledge financial support from MICINN (No. TEC2010-10804-E) and MINECO (Nos. TEC2012-31145 and CTQ2012-37573-C02-02). A.B. acknowledges support from the EAGLES Program.

ABBREVIATIONS

EOT = extraordinary optical transmission
SP = surface plasmon
SPP = surface plasmon polariton
SPR = surface plasmon resonance
RI = refractive index
DIW = deionized water
IPA = isopropyl alcohol
EBL = electron beam lithography
ICP = inductively coupled plasma
SEM = scanning electron microscopy
HMDS = 1,1,1,3,3,3-hexamethyldisilazane

REFERENCES

(1) Wood, R. W. *Proc. Phys. Soc., London* **1902**, *18*, 269−275.
(2) Bethe, H. A. *Phys. Rev.* **1944**, *66*, 163−182.
(3) Ebbesen, T. W.; Lezec, H. J.; Ghaemi, H. F.; Thio, T.; Wolff, P. A. *Nature* **1998**, *391*, 667−669.
(4) Ghaemi, H. F.; Thio, T.; Grupp, D. E.; Ebbesen, T. W.; Lezec, H. J. *Phys. Rev. B* **1998**, *58*, 6779−6782.
(5) Grupp, D. E.; Lezec, H. J.; Thio, T.; Ebbesen, T. W. *Adv. Mater.* **1999**, *11*, 860−862.
(6) Pines, D. *Rev. Mod. Phys.* **1956**, *28*, 184−198.
(7) Lal, S.; Link, S.; Halas, N. J. *Nat. Photonics* **2007**, *1*, 641−648.
(8) Zhang, J.; Zhang, L.; Xu, W. *J. Phys. D: Appl. Phys.* **2012**, *45*, 113001.
(9) Nice, E. C.; Catimel, B. *BioEssays* **1999**, *21*, 339−352.
(10) Homola, J. *Anal. Bioanal. Chem.* **2003**, *377*, 528−539.
(11) Lindquist, N. C.; Nagpal, P.; McPeak, K. M.; Norris, D. J.; Oh, S.-H. *Rep. Prog. Phys.* **2012**, *75*, 036501.
(12) Homola, J.; Yee, S. S.; Gauglitz, G. *Sens. Actuators, B* **1999**, *54*, 3−15.
(13) White, I. M.; Fan, X. *Optics Express* **2008**, *16*, 1020−1028.
(14) Abbas, A.; Linman, M. J.; Cheng, Q. *Biosens. Bioelectron.* **2011**, *26*, 1815−1824.
(15) Šípová, H.; Homola, J. *Anal. Chim. Acta* **2013**, *773*, 9−23.
(16) Couture, M.; Zhao, S. S.; Masson, J. F. *Phys. Chem. Chem. Phys.* **2013**, *15*, 11190−11216.
(17) Preechaburana, P.; Gonzalez, M. C.; Suska, A.; Filippini, D. *Angew. Chem., Int. Ed.* **2012**, *51*, 11585−11588.
(18) Popov, E.; Nevière, M.; Enoch, S.; Reinisch, R. *Phys. Rev. B* **2000**, *62*, 16100−16108.
(19) Martín-Moreno, L.; García-Vidal, F. J.; Lezec, H. J.; Pellerin, K. M.; Thio, T.; Pendry, J. B.; Ebbesen, T. W. *Phys. Rev. Lett.* **2001**, *86*, 1114−1117.
(20) Barnes, W. L.; Dereux, A.; Ebbesen, T. W. *Nature* **2003**, *424*, 824−830.
(21) Lezec, H. J.; Thio, T. *Opt. Express* **2004**, *12*, 3629−3651.
(22) Degiron, A.; Ebbesen, T. W. *J. Opt. A: Pure Appl. Opt.* **2005**, *7*, 90−96.
(23) Ozbay, E. *Science* **2006**, *311*, 189−193.
(24) Ruan, Z.; Qiu, M. *Phys. Rev. Lett.* **2006**, *96*, 233901.
(25) Genet, C.; Ebbesen, T. W. *Nature* **2007**, *445*, 39−46.
(26) Pacifici, D.; Lezec, H. J.; Sweatlock, L. A.; Walters, R. J.; Atwater, H. A. *Opt. Express* **2008**, *16*, 9222−9238.
(27) Liu, H.; Lalanne, P. *Nature* **2008**, *452*, 728−731.
(28) Garcia-Vidal, F. J.; Martin-Moreno, L.; Ebbesen, T. W.; Kuipers, L. *Rev. Mod. Phys.* **2010**, *82*, 729−787.
(29) Couture, M.; Live, L. S.; Dhawan, A.; Masson, J. F. *Analyst* **2012**, *137*, 4162−4170.
(30) Brolo, A. G.; Gordon, R.; Leathem, B.; Kavanagh, K. L. *Langmuir* **2004**, *20*, 4813−4815.
(31) Stark, P. R. H.; Halleck, A. E.; Larson, D. N. *Methods* **2005**, *37*, 37−47.
(32) De Leebeeck, A.; Kumar, L. K.; de Lange, V.; Sinton, D.; Gordon, R.; Brolo, A. G. *Anal. Chem.* **2007**, *79*, 4094−4100.
(33) Schatz, G. C.; McMahon, J. M.; Gray, S. K. *Proc. SPIE* **2007**, *6641*, 664103.
(34) McMahon, J. M.; Henzie, J.; Odom, T. W.; Schatz, G. C.; Gray, S. K. *Opt. Express* **2007**, *15*, 18119−18129.
(35) Stewart, M. E.; Anderton, C. R.; Thompson, L. B.; Maria, J.; Gray, S. K.; Rogers, J. A.; Nuzzo, R. G. *Chem. Rev.* **2008**, *108*, 494−521.
(36) Sharpe, J. C.; Mitchell, J. S.; Lin, L.; Sedoglavich, N.; Blaikie, R. J. *Anal. Chem.* **2008**, *80*, 2244−2249.
(37) Gordon, R.; Sinton, D.; Kavanagh, K. L.; Brolo, A. G. *Acc. Chem. Res.* **2008**, *41*, 1049−1057.
(38) Valsecchi, C.; Brolo, A. G. *Langmuir* **2013**, *29*, 5638−5649.
(39) Escobedo, C. *Lab Chip* **2013**, *13*, 2445−2463.
(40) Cervantes Tellez, G. A.; Hassan, S.; Tait, R. N.; Berini, P.; Gordon, R. *Lab Chip* **2013**, *13*, 2541−2546.
(41) Nakamoto, K.; Kurita, R.; Niwa, O.; Fujii, T.; Nishida, M. *Nanoscale* **2011**, *3*, 5067−5075.
(42) Jia, P.; Jiang, H.; Sabarinathan, J.; Yang, J. *Nanotechnology* **2013**, *24*, 195501 (1-6).
(43) Chang, Y. K.; Lou, Z. X.; Chang, K. D.; Chang, C. W. *Opt. Express* **2013**, *21*, 1804−1811.
(44) Yang, J. -C.; Ji, J.; Hogle, J.M.; Larson, D.N. *Biosens. Bioelectron.* **2009**, *24*, 2334−2338.
(45) Rodrigo, S. G.; García-Vidal, F. J.; Martín-Moreno, L. *Phys. Rev. B* **2008**, *77*, 075401.
(46) West, P. R.; Ishii, S.; Naik, G. V.; Emani, N. K.; Shalaev, V. M.; Boltasseva, A. *Laser Photonics Rev.* **2010**, *4*, 795−808.

(47) Zhang, X.; Zhao, J.; Whitney, A. V.; Elam, J. W.; Van Duyne, R. P. *J. Am. Chem. Soc.* **2006**, *128*, 10304−10309.
(48) Im, H.; Lindquist, N. C.; Lesuffleur, A.; Oh, S.-H. *ACS Nano* **2010**, *4*, 947−954.
(49) *Gold, Silver, Precious & Industrial Metals Prices−Bloomberg*. Available via the Internet at http://www.bloomberg.com/markets/commodities/futures/metals (accessed Sept. 20, 2013).
(50) Langhammer, C.; Schwind, M.; Kasemo, B.; Zorić, I. *Nano Lett.* **2008**, *8*, 1461−1471.
(51) Su, W.; Zheng, G.; Li, X. *Opt. Commun.* **2012**, *285*, 4603−4607.
(52) Yokogawa, S.; Burgos, S.P.; Atwater, H.A. *Nano Lett.* **2012**, *12*, 4349−4354.
(53) Greenwood, N. N.; Earnshaw, A. *Chemistry of the Elements*, 2nd Edition; Butterworth-Heinemann: Oxford, U.K., 1997; Chapter 7.
(54) Herranz, S.; Marciello, M.; Olea, D.; Hernández, M.; Domingo, C.; Vélez, M.; Gheber, L. A.; Guisán, J. M.; Moreno-Bondi, M. C. *Anal. Chem.* **2013**, *85*, 7060−7068.
(55) *Rsoft Products—Synopsis Optical Solutions*. Available via the Internet athttp://optics.synopsys.com/rsoft (accessed Sept. 20, 2013).
(56) Lee, S. H.; Johnson, T. W.; Lindquist, N. C.; Im, H.; Norris, D. J.; Oh, S.-H. *Adv. Funct. Mater.* **2012**, *22*, 4439−4446.
(57) Pang, L.; Hwang, G. M.; Slutsky, B.; Fainman, Y. *Appl. Phys. Lett.* **2007**, *91*, 123112.
(58) Yanik, A. A.; Huang, M.; Artar, A.; Chang, T.-Y.; Altug, H. *Appl. Phys. Lett.* **2010**, *96*, 021101.
(59) Wright, J. B.; Cicotte, K. N.; Subramania, G.; Dirk, S. M.; Brener, I. *Opt. Mater. Express* **2012**, *2*, 1655−1662.
(60) Im, H.; Sutherland, J. N.; Maynard, J. A.; Oh, S. H. *Anal Chem.* **2012**, *84*, 1941−1947.